Electrochimica Acta 116 (2014) 355–365

Contents lists available at ScienceDirect

Electrochimica Acta

journal homepage: www.elsevier.com/locate/electacta

# Application of transient analysis using Hilbert spectra of electrochemical noise to the identification of corrosion inhibition

A.M. Homborg[a], E.P.M. van Westing[b], T. Tinga[c], G.M. Ferrari[d], X. Zhang[d], J.H.W. de Wit[e], J.M.C. Mol[e,*]

[a] Royal Netherlands Navy, Naval Maintenance and Sustainment Agency, P.O. Box 505, 1780AM Den Helder, The Netherlands
[b] Tata Steel, Wenckebachstraat, 1951JZ, Velsen Noord, The Netherlands
[c] Netherlands Defence Academy, P.O. Box 10000, 1780CA Den Helder, The Netherlands
[d] TNO Maritime Materials Performance Centre, P.O. Box 505, 1780AM Den Helder, The Netherlands
[e] Delft University of Technology, Department of Materials Science and Engineering, Mekelweg 2, 2628CD Delft, The Netherlands

ARTICLE INFO

*Article history:*
Received 30 August 2013
Received in revised form
12 November 2013
Accepted 14 November 2013
Available online 26 November 2013

*Keywords:*
Electrochemical noise
Transient analysis
Hilbert spectra
Localized corrosion
Corrosion inhibition

ABSTRACT

This study validates the ability of Hilbert spectra to investigate transients in an electrochemical noise signal for an aqueous corrosion inhibition process. The proposed analysis procedure involves the identification and analysis of transients in the electrochemical current noise signal. Their decomposition into instantaneous frequencies in a Hilbert spectrum allows detection of changes in corrosion characteristics, i.e. the evolution of corrosion inhibition with time. The effectiveness of the proposed analysis procedure is investigated for AA2024-T3 exposed to aqueous $10^{-1}$ M NaCl solutions with or without the addition of Ce ions at various concentrations. Examination of specific features in the electrochemical noise signals shows the presence of three characteristic regions, which represent surface activity regimes ranging from active (localized) corrosion to the inhibited state. Hilbert spectra of the electrochemical current noise signals allow identification of transients occurring in these successive regions.

The analysis procedure introduced in this work yields improved applicability of electrochemical noise measurements for the identification of an inhibition effect in corrosion processes.



## 1. Introduction

Electrochemical noise (EN) consists of spontaneous fluctuations in current and potential, generated by charge transfer reactions that arise from electrochemical metal dissolution processes. It has long been the conviction of many researchers that EN contains valuable information about the underlying corrosion processes. Hladky and Dawson [1,2] reported on their investigations on characteristic fluctuations in the electrochemical potential noise (EPN), generated by the occurrence of localized corrosion. These characteristic fluctuations are defined as transients. Transients in the electrochemical current noise (ECN) signal are often accompanied by transients in the EPN signal [3,4]. Characterization of localized corrosion processes can be regarded as the most interesting application of electrochemical noise measurements (ENM), which is also important for corrosion monitoring [5–10].

For the purpose of characterization of localized corrosion processes through EN signals, many data analysis procedures exist of which the most common are fast Fourier transform and discrete wavelet transform. However, fast Fourier transform is strictly spoken not suitable for the analysis of EN, since corrosion processes are typically nonstationary, a property that is required for data analysis in the frequency domain. A separate procedure is necessary to remove its direct current (DC) drift component and to make an EN signal appear stationary. An approach to define a reliable DC drift component using empirical mode decomposition and wavelet transform is presented by the authors in an earlier work [11]. In addition, the interpretation of specific features (e.g. the roll-off slope) in the resulting power spectral density plot and its relation to the prevalent corrosion mechanism can be considered controversial [3,12–17].

Discrete wavelet transform allows investigation of the distribution of the energy present in a (nonstationary) EN signal over several timescales in an energy distribution plot. However, the separation of the frequency domain into so-called scales instead of real instantaneous frequencies does not result in the desired direct frequency decomposition of the data at any given moment in time.

An interesting approach to distinguish local frequency characteristics of an EN signal is the application of the Hilbert-Huang

* Corresponding author. Tel.: +31 15 278 67 78.
*E-mail addresses:* Axel.Homborg@tno.nl (A.M. Homborg), Erik.van-Westing@tatasteel.com (E.P.M. van Westing), T.Tinga@nlda.nl (T. Tinga), Gabriele.Ferrari@tno.nl (G.M. Ferrari), Xiaolong.Zhang@tno.nl (X. Zhang), J.H.W.DeWit@tudelft.nl (J.H.W. de Wit), J.M.C.Mol@tudelft.nl (J.M.C. Mol).

0013-4686/$ – see front matter © 2013 Elsevier Ltd. All rights reserved.
http://dx.doi.org/10.1016/j.electacta.2013.11.084

transform as was first proposed by Huang et al. [18]. This transform is based on the assumption that any signal consists of multiple characteristic scales, or intrinsic modes of oscillation, each superposed on another. These so-called intrinsic mode functions are based on the local properties of the signal and can be identified empirically by their characteristic time scales through empirical mode decomposition. Intrinsic mode functions could be considered as a more general case of simple harmonic functions, however in close relation with the physical characteristics of the system under investigation due to the specific nature of empirical mode decomposition [19]. The basis of this technique is derived directly from the data itself, making the empirical mode decomposition flexible and adaptive [18,20–22]. A detailed description of the empirical mode decomposition and Hilbert-Huang transform procedure is reported by the authors in prior work [23], where the use of Hilbert spectra for the analysis of EN signals under open-circuit conditions has been proposed in corrosion studies. It was shown that Hilbert spectra enabled to distinguish between different corrosion characteristics [23]. Regarding the interpretation of EN signals, this ability makes the Hilbert-Huang transform a valuable data analysis technique.

The frequency contribution of individual transients yields specific signatures, or 'fingerprints', in the Hilbert spectrum. In earlier work, the principle of transient analysis through Hilbert spectra of EN signals has been presented for metastable pitting corrosion processes on stainless steel for which the characteristics do not change over the duration of the measurements [24]. Interestingly, analysis of the instantaneous frequencies contributing to the transients in an EN signal also enables to detect changes in corrosion characteristics. It was early recognized that the investigation of transients present in the EN signal is essential to understand the corrosion characteristics of aluminium [25]. In this work the principle of transient analysis applied to an aqueous corrosion inhibition process is therefore illustrated by the Ce-based inhibition of AA2024-T3. In order to differentiate between changing corrosion characteristics of the inhibition process, visual investigation of transient information present in these complex EN signals is not straightforward. This gives rise to the need of an adaptive analysis method that allows detection of the changes in the inhibition process. It should be noted that while the original time signatures from metastable pitting are better reported and discussed, little understanding on the signatures of other forms of localized corrosion processes such as pitting growth, crevice corrosion or galvanic corrosion has been achieved to date.

AA2024 consists of an Al matrix with second phase intermetallic particles, many of which contain Cu and are primarily involved in the localized corrosion of AA2024-T3 [26–30]. This can occur either at isolated particles or in clusters of multiple particles [29]. Two types of intermetallic particles can be distinguished, namely those containing Al-Cu(-Mg) or Al-Cu-Fe-Mn(-Si) [31–33]. The most numerous are $Al_2CuMg$ (S-phase) particles, belonging to the first type [28,34]. Except for the S-phase particles, intermetallic particles contain elements that are more noble than the Al matrix, therefore acting as cathodic sites [30,35].

Corrosion inhibition of AA2024-T3 by the commonly used chromate-based inhibitors can be quite effective [36]. A suitable alternative to the commonly used Cr(VI) inhibitor can be e.g. to use lanthanide salts as an ecological substitute [37–43].

The process of inhibition is studied quite thoroughly by others [37–43]. The main contribution of this work is the introduction of transient analysis through Hilbert spectra of EN signals for the investigation of an aqueous corrosion inhibition process. The proposed analysis procedure involves the identification and analysis of the instantaneous frequency composition of transients in the ECN signal. The benefits of the proposed analysis method are supported by visual inspection of the EN signals in the time domain, microscopic observations and literature.

## 2. Experimental

### 2.1. Materials and experimental set-up

The measurements were performed in a conventional three-electrode configuration under open-circuit conditions, requiring two nominally identical AA2024-T3 working electrodes. The measurement setup and electrochemical cell configuration is identical to the one described earlier [23].

The working electrodes were partly coated with an epoxy primer to prevent crevice corrosion and were embedded in coupons using an epoxy resin. Only a well-defined area of 0.05 $cm^2$ of each working electrode was exposed to the electrolyte. The working electrodes were wet ground using up to 4000-grit SiC paper. After rinsing with demineralized water and microscopic inspection for irregularities they were stored under ambient conditions at 20 °C for 24 h. The reference electrode used was a Radiometer analytical Red Rod type REF201 (Ag/AgCl/sat. KCl: 207 mV vs. SHE). The electrolytes used were aqueous NaCl solutions made from demineralised water and analytical grade reagent. These were either used in that composition, or prepared with the addition of $10^{-2}$ to $10^{-5}$ M $CeCl_3 \bullet 7H_2O$. The applied experimental procedure is shown in Fig. 1.

All solutions were open to air. The duration of each exposure to the electrolyte was 14500 s, equal to the duration of each measurement. For each measurement containing $10^{-2}$ to $10^{-5}$ M $CeCl_3 \bullet 7H_2O$, after another 24 hours in ambient air an additional measurement of again 14500 s was performed in an electrolyte containing only $10^{-1}$ M NaCl.

The electrochemical cells were placed in a Faradaic cage to avoid electromagnetic disturbance from external sources. The ambient temperature was controlled at 20 °C. The samples were microscopically inspected afterwards using a Reichert MEF4 M optical microscope with maximum magnification of 1000x. All measurements were performed at least in triplicate.

Current and potential signals were recorded using a Compactstat from Ivium Technologies working as zero resistance ammeter and potentiometer, controlled by a Windows-based PC running dedicated software. The sampling frequency used for the measurements described in this work was 20 Hz. A low-pass filter of 10 Hz (which is the Nyquist frequency at this sampling rate) was applied during data recording. It was verified that instrumental noise generated by the measuring equipment did not affect the measurements. This is described in detail in an earlier paper by the authors [23]. The maximum range of the zero resistance ammeter was automatically determined during the measurements, depending on the dynamic range of the ECN signal locally, with a lower limit of 10 nA and an upper limit of 1 μA. The maximum range of the potentiometer was set at 1 V.

The data were processed using Matlab from MathWorks. The empirical mode decomposition and the Hilbert-Huang transform were calculated using a publicly available Matlab procedure from Rilling et al. [44,45].

### 2.2. Transient analysis

In order to differentiate between changing corrosion characteristics of an inhibition process, visual investigation of transient information present in the complex EN signals is not straightforward. Therefore, in order to obtain information about the localized corrosion processes, the corresponding transients in the EN signals are identified and decomposed into their instantaneous frequencies using Hilbert spectra. The process of transient analysis consists of two steps. First the areas in a Hilbert spectrum corresponding to the occurrence of individual transients are defined. Subsequently, only the amplitudes of the instantaneous frequencies present in

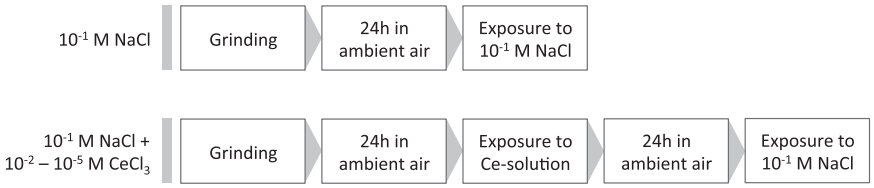


**Fig. 1.** Experimental procedure.

these areas are averaged, in order to obtain the frequency behaviour of the corrosion processes contributing to the overall ECN signal. In this way, good discrimination between different corrosion processes can be obtained and, moreover, any instantaneous frequency information present in between the areas of interest (where no transients occur) is neglected.

An example of the procedure of transient analysis for a corrosion inhibition process is provided in the next section.

## 3. Results and discussion

### 3.1. Visual observation

Fig. 2a-e show micrographs in different magnifications of a measurement of AA2024-T3 exposed to $10^{-1}$ M NaCl with $10^{-2}$ M $CeCl_3 \cdot 7H_2O$ for a duration of 14500 s, where inhibition was observed within the duration of the measurement. Fig. 2f-h show micrographs of the same sample area after the second measurement, now exposed to $10^{-1}$ M NaCl without the addition of $CeCl_3 \cdot 7H_2O$ for a duration of 14500 s, in conformity with the experimental procedure shown in Fig. 1. The reason for this second exposure of the same sample is explained in the next subsection.

The inhibition process of a Ce-based inhibitor is explained through the increased pH near the cathodic sites [46,47]. It is likely that a combination of 3-valent Ce ($Ce(OH)_3$) and 4-valent Ce (less soluble $Ce(OH)_4$ or $CeO_2$) precipitates at cathodic particles [46–48]. This new layer forms an increased barrier for (and thus inhibits) the cathodic processes [35,39,46,47,49,50]. In addition, further dissolution of Al and Mg from these intermetallics is reduced [35]. Due to this inhibition the deposition of Ce also decreases, which implies a self-regulating inhibition process [50].

After the first measurement, including $10^{-2}$ M $CeCl_3 \cdot 7H_2O$, indeed no significant corrosion attack on the surface of the working electrode areas was observed. This is visible when comparing Fig. 2a and 2b with 2c and 2d, and by the further enlargement shown in Fig. 2e. After the second measurement however, involving only $10^{-1}$ M NaCl, at the locations of the same intermetallic particles noticeable corrosion attack is visible. This is shown in Fig. 2f-h: some intermetallic particles are partly dissolved. In most cases however, the aluminium matrix around intermetallic particles was attacked.

Fig. 3 shows micrographs in different magnifications of a measurement of AA2024-T3 exposed to $10^{-1}$ M NaCl for a duration of 14500 s, i.e. without being exposed to a certain concentration of $CeCl_3 \cdot 7H_2O$ beforehand.

In these micrographs a clear corrosion attack is visible at or near the locations of intermetallic particles. In many cases characteristic rings were observed around intermetallic particles. The two rings visible in Fig. 3b are further enlarged in Fig. 3c-e. These rings of corrosion product were also observed by Glenn et al. [51]. They indicate a stable pitting process involving clusters of intermetallic particles located near their centre [29,50,51]. Fig. 4 shows a ring

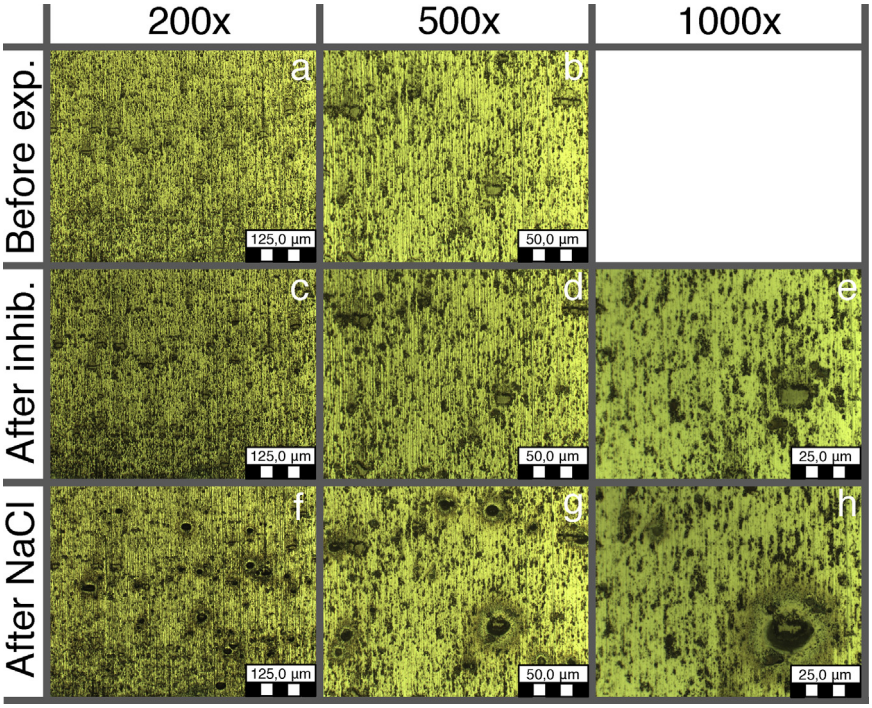


**Fig. 2.** a-e Micrographs of an example measurement of AA2024-T3 exposed to $10^{-1}$ M NaCl with $10^{-2}$ M $CeCl_3 \cdot 7H_2O$ for a duration of 14500 s. Figure 2f-h Micrographs of the second measurement on the same sample, exposed to $10^{-1}$ M NaCl without the addition of $CeCl_3 \cdot 7H_2O$ for a duration of 14500 s.

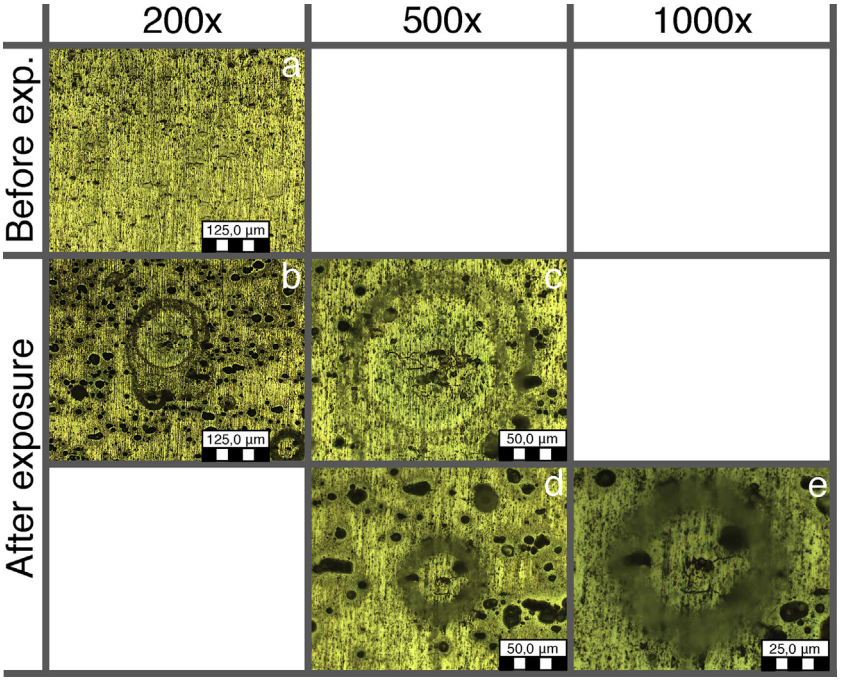


**Fig. 3.** Micrographs of an example measurement of AA2024-T3 exposed to $10^{-1}$ M NaCl for a duration of 14500 s.

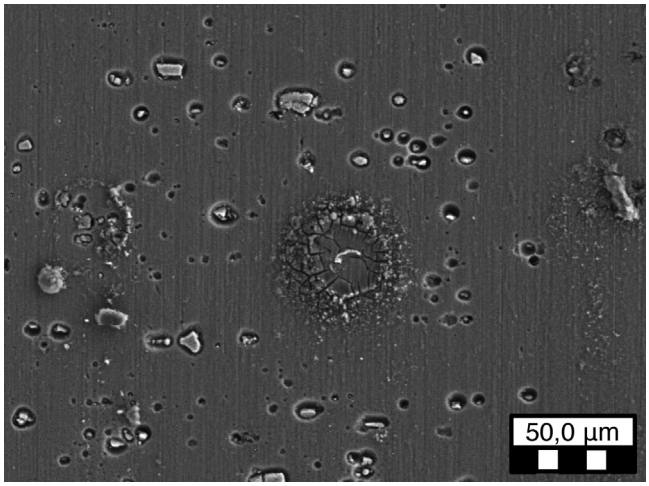


**Fig. 4.** SEM Micrograph of an example measurement of AA2024-T3 exposed to $10^{-1}$ M NaCl for a duration of 14500 s.

of corrosion product on one of the working electrode surfaces in a SEM micrograph.

### 3.2. EN signal analysis

In this subsection, the instantaneous frequency information in the Hilbert spectra, combined with visual observations of the ECN and EPN signals and literature, will be applied to analyze the Ce inhibition process of AA2024-T3.

For two concentrations, $10^{-2}$ and $10^{-3}$ M $CeCl_3 \cdot 7H_2O$, a decrease in the number of transients, the change in instantaneous frequency behaviour (both visible in the Hilbert spectra discussed later) and the absence of corrosion attack at the working electrode surfaces after exposure indicated that inhibition occurred within the timeframe of the measurements. This was however not the case for all measurements at these concentrations, since in some cases inhibition took more time to become effective. In addition, for the measurements that did show inhibition within this timeframe, the time until inhibition became effective varied between 2500 s and 12000 s. Differences in inhibition behaviour between otherwise identical measurements can be expected. Firstly, differences in surface preparation, that are inevitably present, however small, could affect the stability of the oxide film [47]. The location of active and passive sites at the AA2024-T3 surface is also assumed to change continuously over time [52]. Furthermore, intermetallic particles other than S-phase particles can vary in composition, which serves as a basis for their classification [28,30]. $10^{-3}$ M $CeCl_3 \cdot 7H_2O$ is considered as the minimum concentration for effective inhibition for the measurements presented in this work. However, it should be noted that the addition of $10^{-4}$ M $CeCl_3 \cdot 7H_2O$ to a $10^{-1}$ M [47] or a 5 x $10^{-2}$ M [50] NaCl background solution has also been proven to provide effective inhibition. In the latter case, inhibition only occurred after longer exposure times. Therefore, in the case of $10^{-4}$ M $CeCl_3 \cdot 7H_2O$, inhibition could still have occurred at a later stage. The concentration of $10^{-5}$ M $CeCl_3 \cdot 7H_2O$ is considered to be too low to act as an effective corrosion inhibitor under these conditions.

The EN signals for inhibition can be divided into three different characteristic regions. These regions represent active corrosion with the onset of inhibition (region 1), inhibition becoming effective (region 2) and the inhibited state (region 3). Their specific features depend on the concentration of $CeCl_3 \cdot 7H_2O$ in the electrolyte and in addition on whether or not inhibition occurred within the timeframe of the measurement. Fig. 5a shows an ECN and EPN signal for the same measurement (in $10^{-1}$ M NaCl with $10^{-2}$ M $CeCl_3 \cdot 7H_2O$) as used for the micrographs of Fig. 2. Fig. 5b shows an ECN and EPN signal for a measurement in $10^{-1}$ M NaCl with $10^{-3}$ M $CeCl_3 \cdot 7H_2O$. The three regions are also indicated in these figures.

As a comparison, Fig. 6 shows an ECN and EPN signal for the same measurement in $10^{-1}$ M NaCl as used for the micrographs of Fig. 3, i.e. without being exposed to a certain concentration of $CeCl_3 \cdot 7H_2O$ beforehand.

The EN signals for the two concentrations of $CeCl_3 \cdot 7H_2O$ are quite similar. Region 1 is characterized by large fluctuations in the EPN signal, in many cases with amplitudes exceeding 200 mV. These large fluctuations in the EPN signal were observed for all

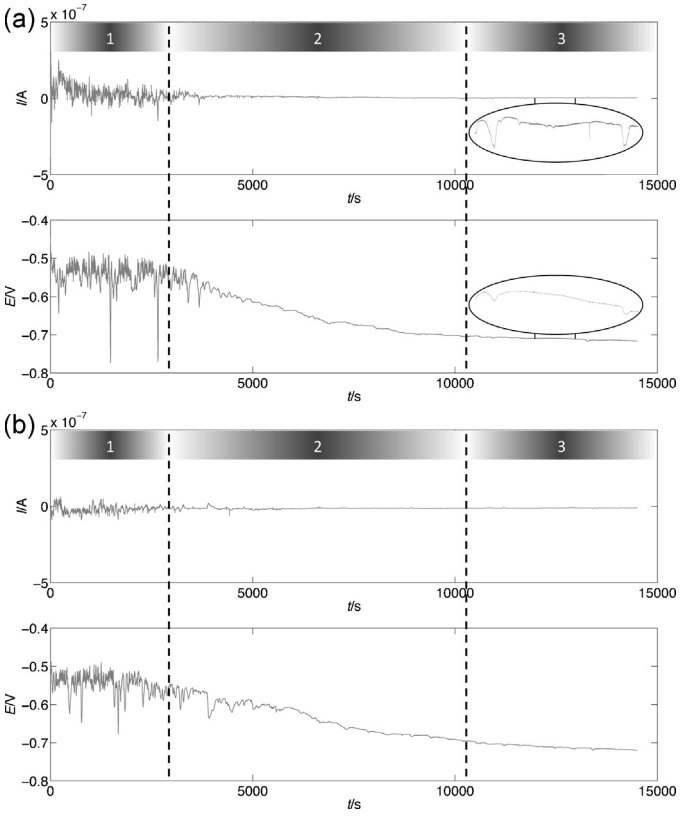


**Fig. 5.** a ECN and EPN signal including inhibition, for AA2024-T3 exposed to $10^{-1}$ M NaCl with $10^{-2}$ M $CeCl_3 \cdot 7H_2O$ for a duration of 14500 s b ECN and EPN signal including inhibition, for AA2024-T3 exposed to $10^{-1}$ M NaCl with $10^{-3}$ M $CeCl_3 \cdot 7H_2O$ for a duration of 14500 s.

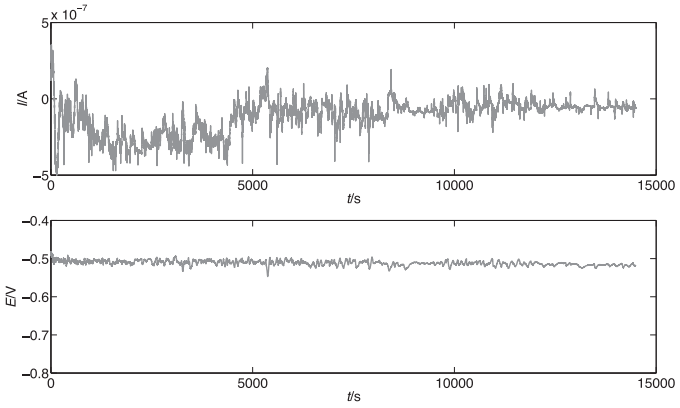


**Fig. 6.** ECN and EPN signal for AA2024-T3 exposed to $10^{-1}$ M NaCl for a duration of 14500 s.

measurements for concentrations containing up to $10^{-4}$ M $CeCl_3 \cdot 7H_2O$. For the measurements in $10^{-5}$ M $CeCl_3 \cdot 7H_2O$ and those in $10^{-1}$ M NaCl only, these large fluctuations were absent. For the cases where inhibition was observed within the timespan of the measurement, these fluctuations were visible in region 1 only, otherwise these existed throughout the entire EPN signal.

In order to verify the nature of these large fluctuations, for each measurement containing $10^{-2}$ to $10^{-5}$ M $CeCl_3 \cdot 7H_2O$, after another 24 hours in ambient air an additional measurement of again 14500 s was performed in an electrolyte containing only $10^{-1}$ M NaCl. In those cases Ce (hydr)oxide was already deposited on the surface and no Ce ions were initially present in the solution. As an example, Fig. 7 shows the ECN and EPN signal for AA2024-T3 exposed to $10^{-1}$

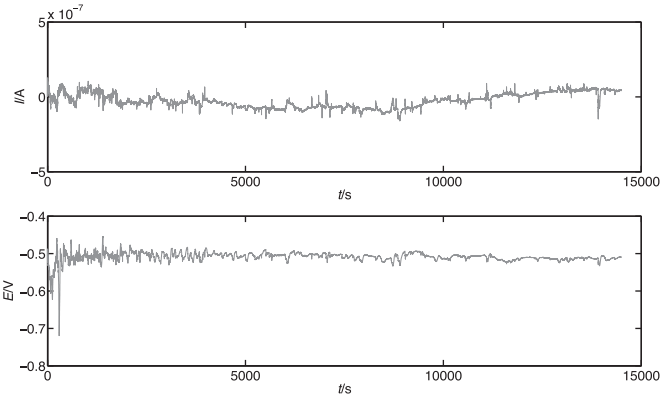


**Fig. 7.** ECN and EPN signal for AA2024-T3 exposed to $10^{-1}$ M NaCl for a duration of 14500 s after an initial exposure to $10^{-1}$ M NaCl with $10^{-2}$ M $CeCl_3 \cdot 7H_2O$ for a duration of 14500 s.

M NaCl for a duration of 14500 s, after an initial exposure to $10^{-1}$ M NaCl with $10^{-2}$ M $CeCl_3 \cdot 7H_2O$ for a duration of 14500 s, of which the EN signals were shown in Fig. 5a.

Fig. 7, without $CeCl_3 \cdot 7H_2O$ present in the electrolyte, shows large fluctuations together with one transient exceeding 200 mV in the EPN signal within the first 1000 s of exposure to NaCl. All second measurements that were performed in electrolytes containing only $10^{-1}$ M NaCl, after measurements in $10^{-2}$ to $10^{-4}$ M $CeCl_3 \cdot 7H_2O$ beforehand, showed large EPN fluctuations within the first 1000 s, all with one or more fluctuations exceeding 200 mV. Subsequently, analogous to the EPN signal shown in Fig. 7, they returned to a similar state as observed for the measurements without Ce (hydr)oxide deposited at the working electrodes or the presence of Ce ions in the electrolyte (as shown in Fig. 6). The observations suggest that these large transients should be attributed to the presence of a not fully intact Ce (hydr)oxide film, leading to local breakdown [33].

During inhibition, the ECN and EPN signals become smoother and the EPN signal shows a negative drift. This is reflected by region 2 in Fig. 5a and 5b. The negative drift of the EPN signal can be explained through the cathodic inhibition process of Ce [37,43,47,50]. The final OCP value of around -700 mV vs. Ag/AgCl is in correspondence with that observed in the work of others [43,50], however at an earlier stage in this case. The reason for this can be the higher concentrations of $CeCl_3 \cdot 7H_2O$ ($10^{-2}$ and $10^{-3}$ M) than compared to the concentration used by García et al. ($10^{-4}$ M), which showed inhibition after longer exposure time.

The OCP values observed for the measurements in $10^{-1}$ M NaCl (around -520 mV vs. Ag/AgCl) were also in accordance with those observed for AA2024-T3 exposed to 5 x $10^{-2}$ M NaCl in the work of García et al. [50] during the first 4 h.

The smoothing of the ECN signal is analogous to a decrease in current density, which is reported by García et al. [47] to occur during inhibition of AA2024-T3. Transients in the ECN and EPN signals, generated by localized corrosion processes, are expected to decrease in amplitude significantly. Note that the fluctuations do not disappear completely, which is visible in Fig. 5a in the magnifications of the third region, between 12000 and 13000 s. The dynamic ranges of these fluctuations are however small, in the order of 1 nA for the ECN signal and 2 mV for the EPN signal. Finally, the drift in the EPN signal disappeared and the ECN signal was close to zero, i.e. both signals indicated that the system reached an inhibited state from the perspective of localized corrosion processes.

Prior to discussion of the Hilbert spectra, an example of the procedure of transient analysis as proposed in this work will be provided. Fig. 8a shows the Hilbert spectrum for the ECN signal shown in Fig. 5a, between 2000 s and 4000 s. Fig. 8b shows the

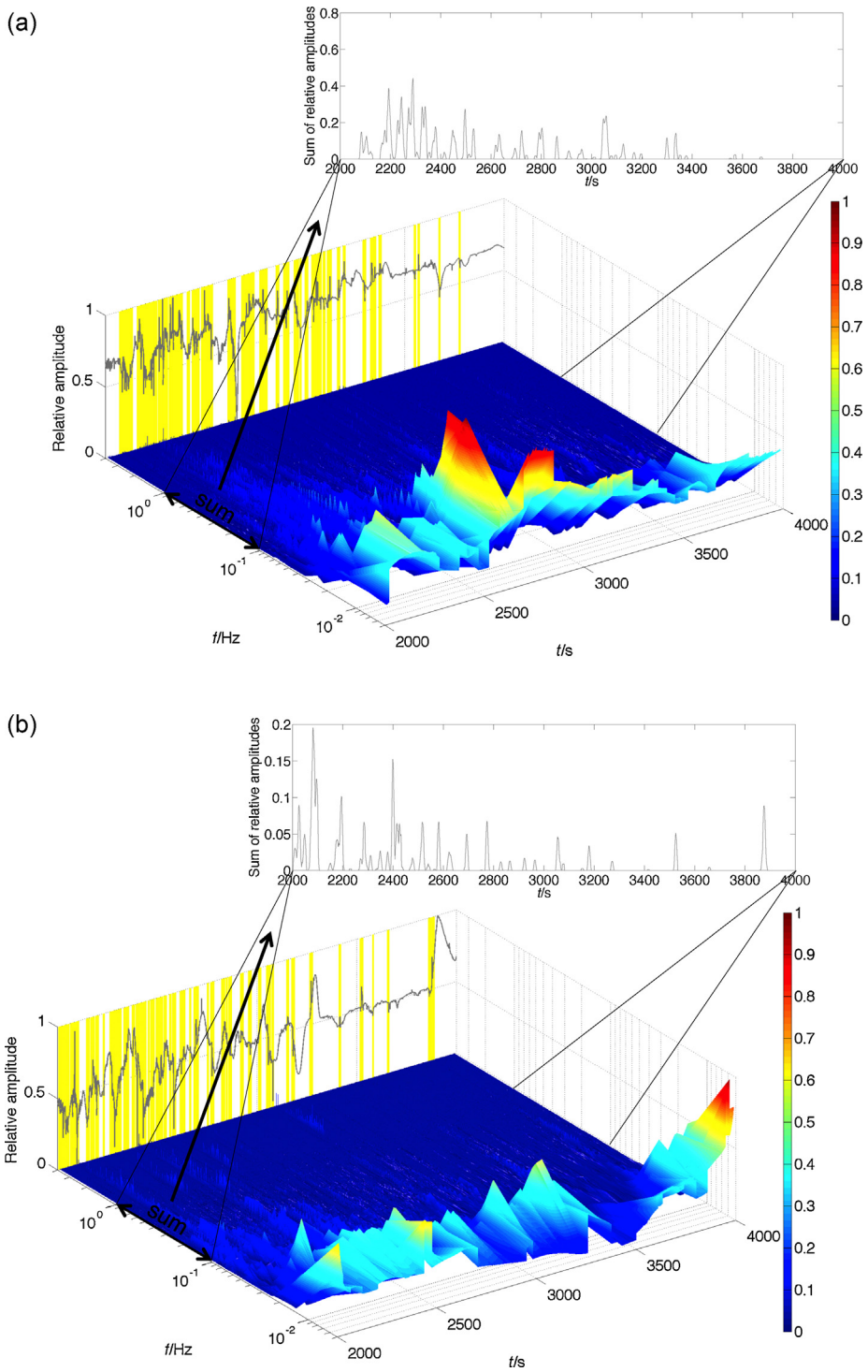


**Fig. 8.** a Hilbert spectrum of the ECN signal of AA2024-T3 exposed to $10^{-1}$ M NaCl with $10^{-2}$ M $CeCl_3 \cdot 7H_2O$, between 2000 s and 4000 s b Hilbert spectrum of the ECN signal of AA2024-T3 exposed to $10^{-1}$ M NaCl with $10^{-3}$ M $CeCl_3 \cdot 7H_2O$, between 2000 s and 4000 s.

Hilbert spectrum for the ECN signal shown in Fig. 5b, in the same time interval. Fig. 9 shows the Hilbert spectrum for the ECN signal shown in Fig. 6, again in the same time interval. The original ECN signals are depicted at the back of the figures with their relative amplitudes. The areas corresponding to the occurrence of transients are highlighted in yellow. Only these areas are analysed in the Hilbert spectrum.

The Hilbert spectra shown in Figures 8a, 8b and 9 will be shown to allow detection of the ECN transients based on their instantaneous frequencies. The process of identification and selection of the areas of interest in the Hilbert spectra and the subsequent analysis of the instantaneous frequencies present in these areas is reported by the authors in prior work [24]. However, in the present work, the first stage of selection of areas of interest is different than proposed earlier [24]. Transients present in the ECN signals typically contain instantaneous frequencies in the range between $10^{-1}$ Hz and 1 Hz. This is illustrated in the top graphs of Figures 8a, 8b and 9, that show the sum of all

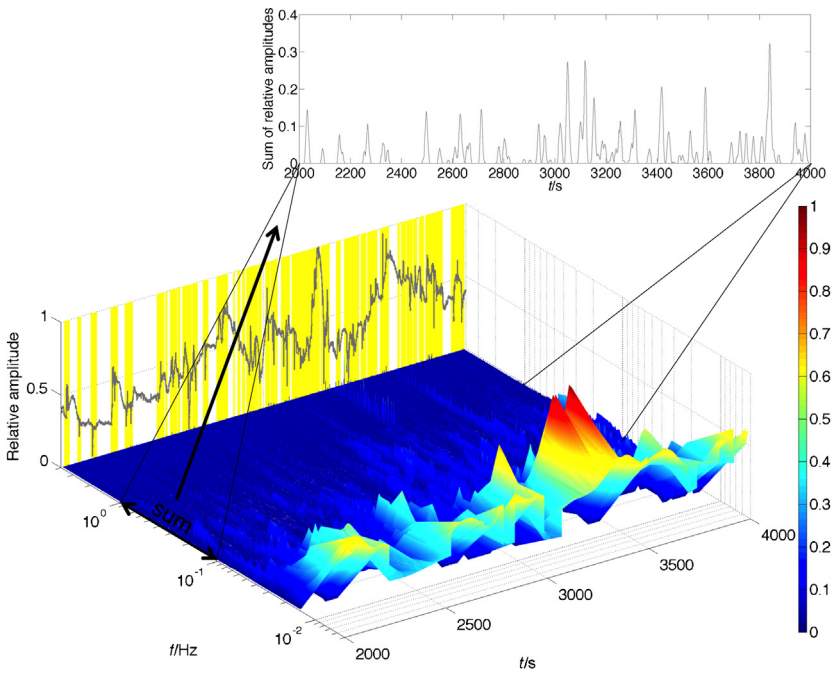


**Fig. 9.** Hilbert spectrum of the ECN signal of AA2024-T3 exposed to $10^{-1}$ M NaCl, between 2000 s and 4000 s.

instantaneous frequency amplitudes in the Hilbert spectra within this frequency range, after removal of the standard deviation and application of a moving average smoothing filter with a specified span of 9x the sampling frequency. Each peak thus corresponds to the instantaneous frequency contributions of a single transient. Transient selection is based on the timespan covered by each individual peak (i.e. its maximum duration at the time axis). This provides an accurate determination of the areas of interest in the Hilbert spectra for the ECN signals as investigated here; for each transient, within its timespan, all instantaneous frequencies are analysed. In Figs. 8a, 8b and 9, the corresponding areas of interest in each Hilbert spectrum are shown in yellow.

To facilitate interpretation of the instantaneous frequency characteristics, their two-dimensional representations are used here. This is the two-dimensional view in the X-Z plane. Any change in instantaneous frequency behaviour (e.g. due to a gradual inhibition process) can be quantified by changes in these two-dimensional representations. Combined with the time-resolved information in the original Hilbert spectra, this is the true added value of the Hilbert spectrum analysis compared to the ECN/EPN signal analysis discussed before.

Now the procedure has been illustrated, the spectra of the different experiments will be discussed.

Fig. 10a and 10b show the two-dimensional representations of the Hilbert spectra of the ECN signal visible in Fig. 5a and 5b, respectively. Hilbert spectra were calculated for 5 successive segments of each 2000 s duration, from t = 0-2000 s (1) to t = 8000-10000 s (5). For each data set a trend line is shown, calculated by a moving average smoothing filter with a specified span of 9 data points.

As a comparison, Fig. 11 shows the two-dimensional representations of the Hilbert spectra of the ECN signal visible in Fig. 6, i.e. a measurement without exposure to $CeCl_3 \cdot 7H_2O$ or presence of deposited Ce (hydr)oxide.

Initially, from 0 s to 4000 s (i.e. Hilbert spectrum 1 and 2) the Hilbert spectra are characterized by a large number of transients (visible in the first part of the Hilbert spectra shown in Fig. 8a and 8b, and also visible in the Hilbert spectrum shown in Fig. 9), for which the decomposition in instantaneous frequencies of the two ECN signals is comparable. In this period, a gradual increase in amplitude is visible with decreasing instantaneous frequencies. Below 5 x $10^{-2}$ Hz, the contribution of instantaneous frequencies is considerably larger.

Pitting corrosion of AA2024-T3 initiates immediately after immersion in an aqueous NaCl electrolyte [34,35]. This process consists of several different stages, including selective dissolution, i.e. dealloying, of the active elements Al and Mg from the constituent particles, amongst others resulting in more noble Cu-rich remnants with a porous structure, and the formation of galvanic couples between the particles and the Al matrix [28,30,34,35,53]. The local cathodic reactions generate significant amounts of $OH^-$ [53]. In a stagnant electrolyte this will lead to a local alkalization near the interface between the Al matrix and an S-phase particle [53]. The Al matrix around the Cu-rich particles starts to dissolve, referred to as trenching [35,54]. This is visible in the micrographs shown in Figures 2f-h and 3. This may develop further and especially in the presence of clusters of S-phase particles and other intermetallic particles at the alloy surface into severe (stable) pitting [29]. The surface of the clusters of particles acts as a net cathode, moving the anode into the surface along the grain boundaries [29]. Corrosion product will deposit around the cluster areas in a ring-shaped morphology [29,50]. These features are also present at the working electrode surfaces shown in Figures. 3 and 4.

Although the ECN signal of AA2024-T3 exposed to $10^{-1}$ M NaCl shows a small decrease in overall amplitudes over the entire measurement (visible in Fig. 6), the relative contribution of instantaneous frequencies remains more or less constant throughout the entire measurement, which is visible in Fig. 11. The Hilbert spectra shown in Fig. 10a and 10b, however, show an increase in relative contribution of high instantaneous frequencies between 4000 s and 6000 s (spectrum 3). Combined with a considerable decrease in the number of transients, this marks the transition between the active and the inhibited state. In order to visualize this, Fig. 12a shows the Hilbert spectrum of the ECN signal shown in Fig. 5a between 4000 s and 6000 s. Fig. 12b shows the Hilbert spectrum of the ECN signal

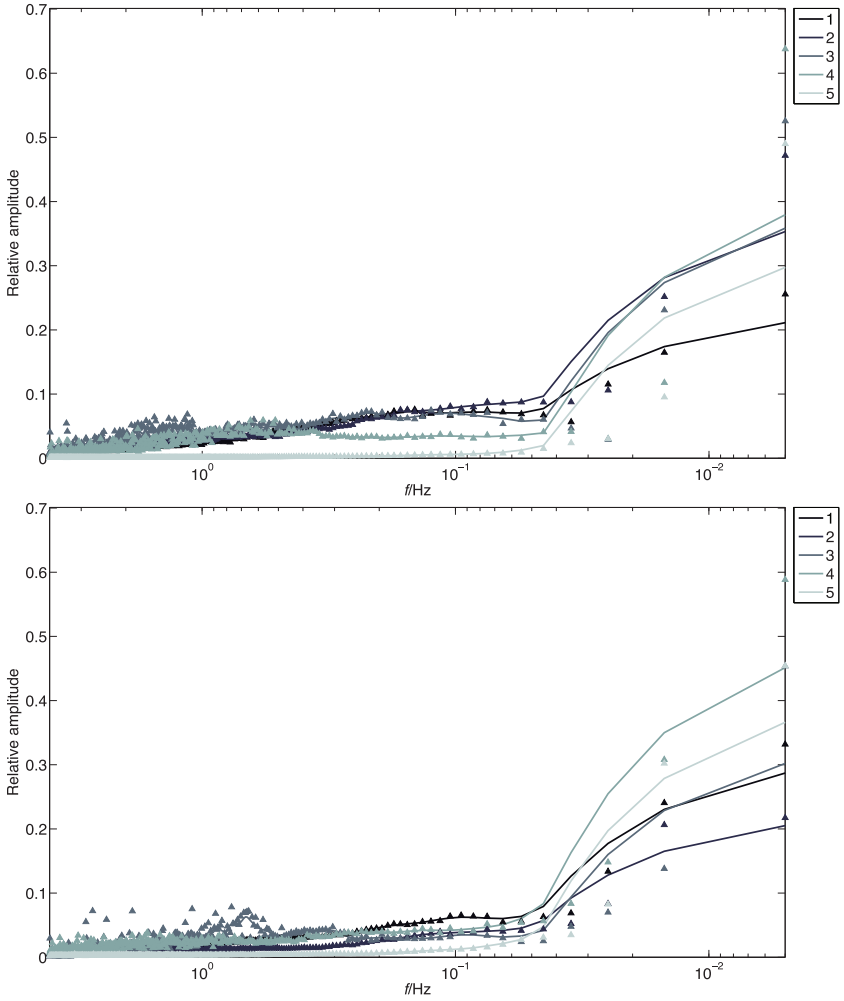


**Fig. 10.** a Two-dimensional representations of the Hilbert spectra of the ECN signal for AA2024-T3 exposed to $10^{-1}$ M NaCl with $10^{-2}$ M $CeCl_3 \bullet 7H_2O$. Hilbert spectra were calculated for 5 successive segments of each 2000 s duration, from t = 0-2000 s (1) to t = 8000-10000 s (5) b Two-dimensional representations of the Hilbert spectra of the ECN signal for AA2024-T3 exposed to $10^{-1}$ M NaCl with $10^{-3}$ M $CeCl_3 \bullet 7H_2O$. Hilbert spectra were calculated for 5 successive segments of each 2000 s duration, from t = 0-2000 s (1) to t = 8000-10000 s (5).

shown in Fig. 5b, in the same time interval. Fig. 13 shows the Hilbert spectrum of the ECN signal shown in Fig. 6, again in the same time interval. The original ECN signals are depicted at the back of the figures with their relative amplitudes.

For the Hilbert spectra shown in Fig. 12a and 12b, compared to their predecessors shown in Fig. 8a and 8b, in this stage fewer transients occur. In the Hilbert spectrum shown in Fig. 13, this decrease in the number of transients is not observed. Compared with the observation from its two-dimensional representation shown in Fig. 11, i.e. that the decomposition in instantaneous frequencies is comparable for all Hilbert spectra throughout the measurement, no significant changes in corrosion characteristics are expected for the corrosion process reflected by the EN signals shown in Fig. 6.

The Hilbert spectrum visible in Fig. 12b shows a relatively large transient at approximately t = 4400 s. By averaging the contribution in instantaneous frequencies of all transients, the domination of the amplitudes of instantaneous frequencies of some (large) transients over those of others can be prevented, which provides the required insensitivity for one or two dominant transients [24].

The high frequency range can be ascribed to spontaneous nucleation and passivation events, whereas fluctuations in the order of several seconds arise from (meta)stable pitting events [26]. Analogous to this, long fluctuations are generated by the slow diffusion processes of oxygen around these active corrosion sites [55].

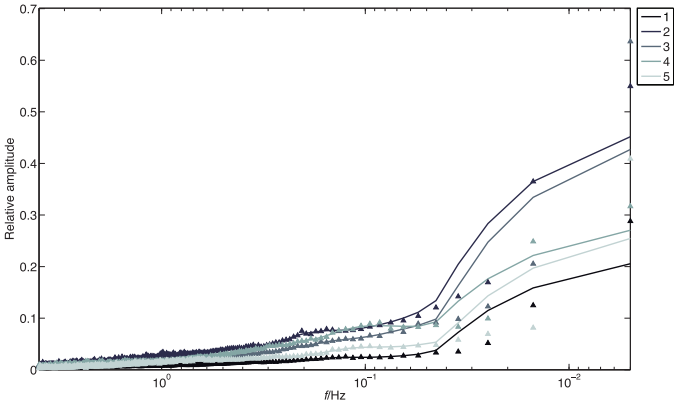


**Fig. 11.** Two-dimensional representations of the Hilbert spectra of the ECN signal for AA2024-T3 exposed to $10^{-1}$ M NaCl. Hilbert spectra were calculated for 5 successive segments of each 2000 s duration, from t = 0-2000 s (1) to t = 8000-10000 s (5).

The Hilbert spectrum shown in Fig. 8a indicates a decreasing intensity across the entire instantaneous frequency range towards 4000 s. In the Hilbert spectra of the ECN signal shown in Fig. 5b, this occurs at a later stage. This can be observed when comparing the Hilbert spectrum shown in Fig. 8b with the one shown in Fig. 12b, where the decrease is visible. The Hilbert spectra in Fig. 12a and

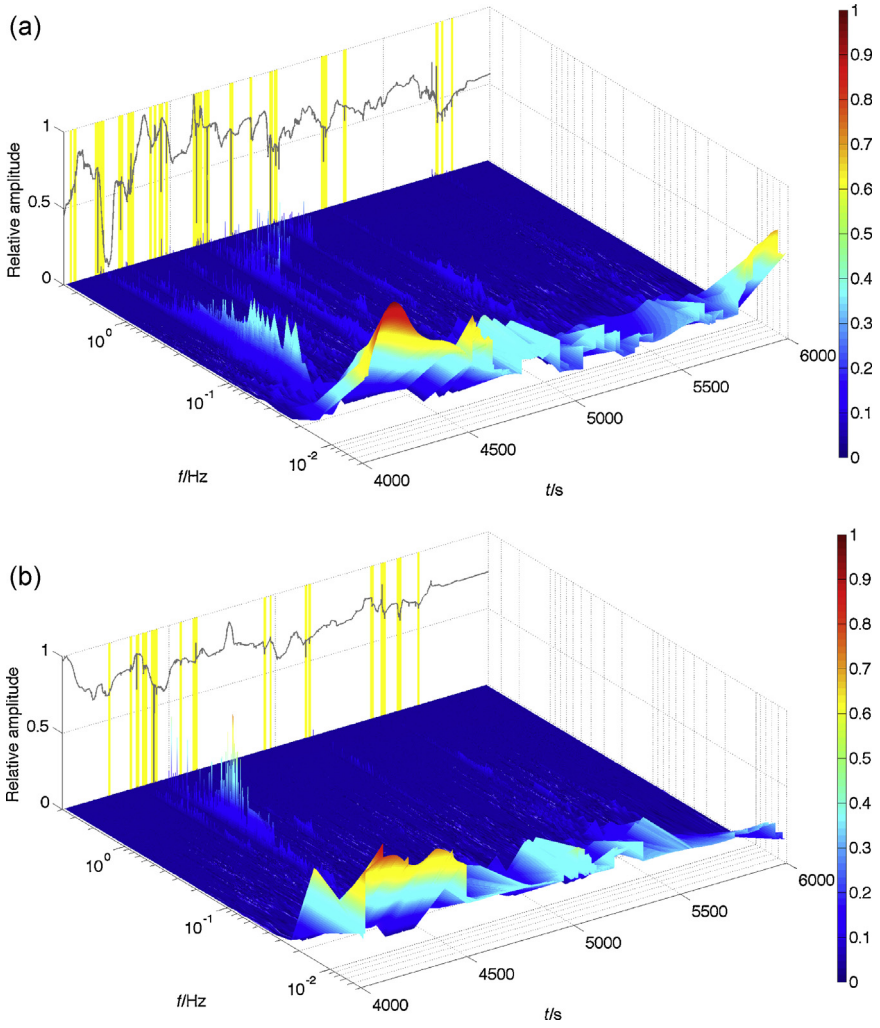


**Fig. 12.** a Hilbert spectrum of the ECN signal of AA2024-T3 exposed to $10^{-1}$ M NaCl with $10^{-2}$ M $CeCl_3 \cdot 7H_2O$, between 4000 s and 6000 s b Hilbert spectrum of the ECN signal of AA2024-T3 exposed to $10^{-1}$ M NaCl with $10^{-3}$ M $CeCl_3 \cdot 7H_2O$, between 4000 s and 6000 s.

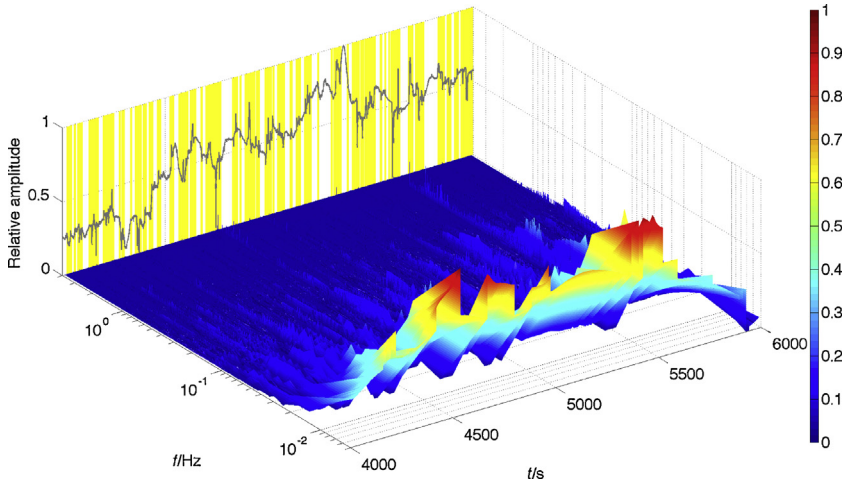


**Fig. 13.** Hilbert spectrum of the ECN signal of AA2024-T3 exposed to $10^{-1}$ M NaCl, between 4000 s and 6000 s.

12b show that the few fast transients present in this segment, with instantaneous frequencies above 5 x $10^{-1}$ Hz, now have a higher relative contribution as compared to the reduced contribution of instantaneous frequencies below 5 x $10^{-2}$ Hz. Still, instantaneous frequencies below 5 x $10^{-2}$ Hz have the largest relative amplitudes, however the absolute intensity of their related diffusion controlled processes has decreased. The reason for this can be the competition between precipitation of Ce (hydr)oxide on the one hand and its breakdown by chloride attack on the other. This gives rise to fast metastable pitting events.

During the next stage towards inhibition (spectrum 4), a decrease of the contribution of instantaneous frequencies across the entire frequency range is visible in Fig. 10a and 10b. Combined with the negative drift in the EPN signal, this indicates the presence of a more robust Ce (hydr)oxide film: both fast metastable pitting events as well as slow oxygen diffusion processes become more inhibited. Subsequently, the final segment shows that when an inhibited (steady) state is reached, almost no metastable pitting events exist anymore. In addition, the final two-dimensional representations of the Hilbert spectra of the ECN signals confirm that a Ce-based inhibitor only inhibits corrosion processes related to the cathodic intermetallic particles: after inhibition, still low frequency information is present in the signal, which indicates that still a general (diffusion controlled) corrosion process is active here. Note that the absolute amplitudes of these large timescale processes have diminished, which is visible in Fig. 5a and 5b by a smooth final part of the ECN signal with fluctuations in the order of 1 nA. Instantaneous frequencies above 5 x $10^{-2}$ Hz (indicative for the competition between chloride attack and formation of the inhibiting layer) are absent here. Therefore, the Hilbert spectra show that for this final segment all instantaneous frequency contribution, however small in the original ECN signal, is in the range below 5 x $10^{-2}$ Hz.

The combination of the range of experiments at different conditions, the associated EN measurements and the knowledge on the processes available in literature strongly support our claim that the proposed method is valuable in distinguishing different stages in a corrosion inhibition process. However, hard evidence can only be obtained when direct in-situ identification of the corrosion process is performed. This type of experiments will therefore have to be performed to further mature the method.

## 4. Conclusions

This study demonstrates the ability of Hilbert spectra to investigate transients in an EN signal for an aqueous corrosion inhibition process. Transient analysis through Hilbert spectra enables the identification of the inhibition process of AA2024-T3 by a Ce-containing solution. Initial examination of specific features in the ECN and EPN signals shows the presence of three characteristic regions, which represent surface activity regimes ranging from active (localized) corrosion to the inhibited state. Hilbert spectra of the ECN signals allow identification of dominant instantaneous frequencies occurring in these successive regions. Combined with microscopic investigation, this can provide time-resolved information about the evolution of the corrosion inhibition from EN signals. Initially, the Hilbert spectra indicate a comparable decomposition in instantaneous frequencies for the AA2024-T3 exposed to a Ce-containing solution as compared to AA2024-T3 exposed to a $10^{-1}$ M NaCl solution. Then the fast competition between precipitation of Ce (hydr)oxide on the one hand and its breakdown by chloride attack on the other becomes visible as a decrease in the number of transients and an increase in relative contribution of instantaneous frequencies above 5 x $10^{-1}$ Hz in this stage. Finally, an inhibited state is reached in which the Hilbert spectrum of the ECN signal indicates that both high and low instantaneous frequencies decrease in amplitude. Both fast metastable pitting events as well as slow oxygen diffusion processes become inhibited, probably due to the presence of a more stable Ce (hydr)oxide film at the surface.

The analysis procedure introduced in this work yields improved applicability of ENM for the identification of an inhibition effect in corrosion processes. By combining transient analysis through Hilbert spectra with visual inspection of the EN signals in the time domain and microscopic observations, on the one hand the effectiveness of the inhibition process could be verified and on the other hand, supported by literature, the nature of the corrosion attack could be explained.

Combined with proper understanding of the physico-chemical process and together with the non-intrusive nature of this measurement technique, this is expected to be valuable for future fully automated detection of corrosion phenomena.

## Acknowledgements

The Naval Maintenance and Sustainment Agency of the Royal Netherlands Navy and TNO Maritime Materials Performance Centre are gratefully acknowledged for enabling this research and accommodating the research work, respectively. Mr Peter Visser from Akzo Nobel Aerospace Coatings is acknowledged for supplying the AA2024-T3 specimens. This research was carried out under project number M32.6.10396 in the framework of the Research Program of the Materials innovation institute M2i (www.m2i.nl).

## References

[1] K. Hladky, J.L. Dawson, Corros. Sci. 21 (1981) 317–322.
[2] K. Hladky, J.L. Dawson, Corros. Sci. 22 (1982) 231–237.
[3] S.W. Kim, H.P. Kim, Corros. Sci. 51 (2009) 191–196.
[4] T. Zhang, Y. Shao, G. Meng, F. Wang, Electrochim. Acta 53 (2007) 561–568.
[5] R.A. Cottis, J. Corros. Sci. Eng. 3 (2000) 1–9.
[6] S.V. Muniandy, W.X. Chew, C.S. Kan, Corros. Sci. 53 (2011) 188–200.
[7] C. Gabrielli, M. Keddam, Corrosion 48 (1992) 794–811.
[8] M. Breimesser, S. Ritter, H. Seifert, T. Suter, S. Virtanen, Corros. Sci. 63 (2012) 129–139.
[9] Q. Hu, G. Zhang, Y. Qiu, X. Guo, Corros. Sci. 53 (2011) 4065–4072.
[10] A. Aballe, M. Bethencourt, F.J. Botana, M. Marcos, J.M. Sánchez-Amaya, Electrochim. Acta 46 (2001) 2353–2361.
[11] A.M. Homborg, T. Tinga, X. Zhang, E.P.M. van Westing, P.J. Oonincx, J.H.W. de Wit, J.M.C. Mol, Electrochim. Acta 70 (2012) 199–209.
[12] J.J. Kim, Mater. Lett. 61 (2007) 4000–4002.
[13] T. Anita, M.G. Pujar, H. Shaikh, R.K. Dayal, H.S. Khatak, Corros. Sci. 48 (2006) 2689–2710.
[14] Y. Tan, Sens. Actuators, B 139 (2009) 688–698.
[15] A. Aballe, M. Bethencourt, F.J. Botana, M. Marcos, Electrochem. Commun. 1 (1999) 266–270.
[16] A. Aballe, M. Bethencourt, F.J. Botana, M. Marcos, Electrochim. Acta 44 (1999) 4805–4816.
[17] R.A. Cottis, Corrosion 57 (2001) 265–285.
[18] N.E. Huang, Z. Shen, S.R. Long, M.C. Wu, H.H. Shih, Q. Zheng, N.C. Yen, C.C. Tung, H.H. Liu, Proc. R. Soc. London 454 (1998) 903–995.
[19] A.D. Veltcheva, C.G. Soares, Applied Ocean Research 26 (2004) 1–12.
[20] N.E. Huang, Z. Shen, S.R. Long, Annu. Rev. Fluid Mech. 31 (1999) 417–457.
[21] Z. Wu, N.E. Huang, Proc. R. Soc. London 460 (2004) 1597–1611.
[22] M. Feldman, Mechanical Systems and Signal Processing 25 (2011) 735–802.
[23] A.M. Homborg, E.P.M. van Westing, T. Tinga, X. Zhang, P.J. Oonincx, G.M. Ferrari, J.H.W. de Wit, J.M.C. Mol, Corros. Sci. 66 (2013) 97–110.
[24] A.M. Homborg, T. Tinga, X. Zhang, E.P.M. van Westing, P.J. Oonincx, G.M. Ferrari, J.H.W. de Wit, J.M.C. Mol, Electrochim. Acta 104 (2013) 84–93.
[25] T. Hagyard, J.R. Williams, Trans. Faraday Soc. 57 (1961) 2288–2294.
[26] A.E. Hughes, N. Birbilis, J.M.C. Mol, S.J. Garcia, X. Zhou, G.E. Thompson, High Strength Al-Alloys: Microstructure, Corrosion and Principles of Protection, in: Z. Ahmad (Ed.), Recent Trends in Processing and Degradation of Aluminium Alloys, InTech, 2011, pp. 223–262.
[27] N.L. Sukiman, X. Zhou, N. Birbilis, A.E. Hughes, J.M.C. Mol, S.J. Garcia, X. Zhou, G.E. Thompson, Durability and Corrosion of Aluminium and Its Alloys: Overview, Property Space, Techniques and Developments, in: Z. Ahmad (Ed.), Aluminium Alloys - New Trends in Fabrication and Applications, InTech, 2012, pp. 57–64.
[28] R.G. Buchheit, R.P. Grant, P.F. Hlava, B. Mckenzie, G.L. Zender, J. Electrochem. Soc. 144 (1997) 2621–2628.
[29] A.E. Hughes, A. Boag, A.M. Glenn, D. McCulloch, T.H. Muster, C. Ryan, C. Luo, X. Zhou, G.E. Thompson, Corros. Sci. 53 (2011) 27–39.
[30] A. Boag, A.E. Hughes, A.M. Glenn, T.H. Muster, D. McCulloch, Corros. Sci. 53 (2011) 17–26.
[31] P. Campestrini, H. Terryn, J. Vereecken, J.H.W.d. Wit, J. Electrochem. Soc. 151 (2004) 359–369.
[32] P. Campestrini, H.W.v. Rooijen, E.P.M.v. Westing, J.H.W.d. Wit, Mater. Corros. 51 (2000) 616–627.
[33] P. Campestrini, H. Terryn, A. Hovestad, J.H.W.d. Wit, Surf. Coat. Technol. 176 (2004) 365–381.
[34] M. Shao, Y. Fu, R. Hu, C. Lin, Mater. Sci. Eng. A344 (2003) 323–327.
[35] K.A. Yasakau, M.L. Zheludkevich, S.V. Lamaka, M.G.S. Ferreira, The Journal of Physical Chemistry B 110 (2006) 5515–5528.
[36] W.J. Clark, J.D. Ramsey, R.L. McCreery, G.S. Frankel, J. Electrochem. Soc. 149 (2002) 179–185.
[37] B.R.W. Hinton, J. Alloys Compd. 180 (1992) 15–25.

[38] A.E. Hughes, D. Ho, M. Forsyth, B.R.W. Hinton, Corrosion Reviews 25 (2007) 591–605.
[39] M. Bethencourt, F.J. Botana, J.J. Calvino, M. Marcos, M.A. Rodríguez-Chacón, Corros. Sci. 40 (1998) 1803–1819.
[40] M. Bethencourt, F.J. Botana, M.A. Cauqui, M. Marcos, M.A. Rodríguez, J.M. Rodríguez-Izquierdo, J. Alloys Compd. 250 (1997) 455–460.
[41] R.L. Twite, G.P. Bierwagen, Prog. Org. Coat. 33 (1998) 91–100.
[42] T.H. Muster, D. Lau, H. Wrubel, N. Sherman, A.E. Hughes, T.G. Harvey, T. Markley, D.L.J. Alexander, P.A. Corrigan, P.A. White, S.G. Hardin, M.A. Glenn, J. Mardel, S.J. Garcia, J.M.C. Mol, Surf. Interface Anal. 42 (2010) 170–174.
[43] T.H. Muster, H. Sullivan, D. Lau, D.L.J. Alexander, N. Sherman, S.J. Garcia, T.G. Harvey, T.A. Markley, A.E. Hughes, P.A. Corrigan, A.M. Glenn, P.A. White, S.G. Hardin, J. Mardel, J.M.C. Mol, Electrochim. Acta 67 (2012) 95–103.
[44] G. Rilling, P. Flandrin, P. Goncalves, IEEE-EURASIP workshop on Nonlinear Signal and Image Processing NSIP-03, Grado, Italy (2003) 1–5.
[45] P. Flandrin, G. Rilling, P. Goncalves, IEEE Signal Processing Letters 11 (2004) 112–114.
[46] E.A. Matter, S. Kozhukharov, M. Machkova, V. Kozhukharov, Corros. Sci. 62 (2012) 22–33.
[47] S.J. García, T.H. Muster, Ö. Özkanat, N. Sherman, A.E. Hughes, H. Terryn, J.H.W. de Wit, J.M.C. Mol, Electrochim. Acta 55 (2010) 2457–2465.
[48] A.J. Davenport, H.S. Isaacs, M.W. Kendig, Corros. Sci. 32 (1991) 653–663.
[49] T.A. Markley, M. Forsyth, A.E. Hughes, Electrochim. Acta 52 (2007) 4024–4031.
[50] S.J. Garcia, T.A. Markley, J.M.C. Mol, A.E. Hughes, Corros. Sci. 69 (2013) 346–358.
[51] A.M. Glenn, T.H. Muster, C. Luo, X. Zhou, G.E. Thompson, A. Boag, A.E. Hughes, Corros. Sci. 53 (2011) 40–50.
[52] D. Battocchi, J. He, G.P. Bierwagen, D.E. Tallman, Corros. Sci. 47 (2005) 1165–1176.
[53] D. Zhu, W.J. van Ooij, Corros. Sci. 45 (2003) 2163–2175.
[54] J.B. Jorcin, C. Blanc, N. Pébère, B. Tribollet, V. Vivier, J. Electrochem. Soc. 155 (2008) C46–C51.
[55] Y. Shi, Z. Zhang, J. Su, F. Cao, J. Zhang, Electrochim. Acta 51 (2006) 4977–4986.